Computing Open-Loop Optimal Control of the q-Profile in Ramp-Up Tokamak Plasmas Using the Minimal-Surface Theory*

XU Chao (许超)[1,2], OU Yongsheng (欧勇盛)[2], Eugenio SCHUSTER[3] and YU Xin (于欣)[4]

[1]The State Key Laboratory of Industrial Control Technology, Zhejiang University, Hangzhou 310027, China
[2]Shenzhen Institutes of Advanced Technology, Chinese Academy of Sciences, Shenzhen 518055, China
[3]Department of Mechanical Engineering & Mechanics, Lehigh University, Bethlehem, PA 18015, USA
[4]Ningbo Institute of Technology, Zhejiang University, Ningbo 315100, China

Abstract The q-profile control problem in the ramp-up phase of plasma discharges is considered in this work. The magnetic diffusion partial differential equation (PDE) models the dynamics of the poloidal magnetic flux profile, which is used in this work to formulate a PDE-constrained optimization problem under a quasi-static assumption. The minimum surface theory and constrained numeric optimization are then applied to achieve suboptimal solutions. Since the transient dynamics is pre-given by the minimum surface theory, then this method can dramatically accelerate the solution process. In order to be robust under external uncertainties in real implementations, PID (proportional-integral-derivative) controllers are used to force the actuators to follow the computational input trajectories. It has the potential to implement in real-time for long time discharges by combining this method with the magnetic equilibrium update.

Keywords: advanced plasma operations, current profile dynamics, optimal control theory, minimal surface equation, differential geometry

PACS: *28.52.Cx, 02.40.-k, 02.60.-x*

DOI: 10.1088/1009-0630/15/5/02

1 Introduction

During the ramp-up phase of a tokamak discharge (Fig. 1), multiple external sources (e.g., Ohmic heating, neutral beam injection, radio frequency) can be used to control the spatial profile of many different plasma variables such as density, temperature, current, and rotation. Transport models usually governed by 1-D nonlinear coupled partial differential equations (PDEs) can be used to predict the plasma dynamics with certain degree of accuracy (e.g., Refs. [1,2]). Strong nonlinearities and model uncertainties add to the complexity of the problem. In addition to that, multi time scale phenomena make the problem even more challenging. For example, the NBI (neutral beam injection) creates high energy particles and is accompanied by the slowing down process, redistribution of the energy with the time scale of energy confinement. These time scales are different from both the particle confinement and the momentum confinement time scales in general. Thus, the approximated method of time scale separation (such as the singular perturbation method [3]) has to be used to decouple various dynamic processes of different time scales.

Different from the prediction problem, where inputs and initial profiles are given to calculate the time response, the control problem is to find admissible inputs that can drive the plasma from given initial profiles to the vicinity of predefined desired profiles. The solution

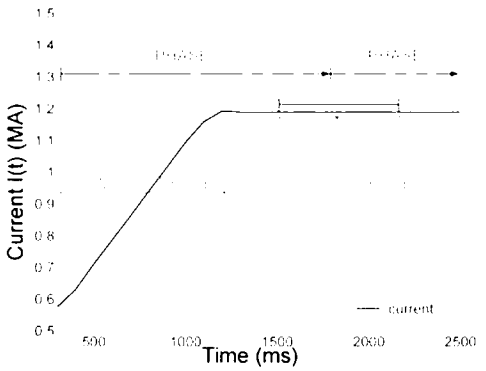

Fig.1 A sample: the total plasma current evolution can be divided in several phases. In this work we focus on phase I, which includes the ramp-up phase and the first part of the flattop phase. The control goal is to drive the magnetic flux profile from some initial arbitrary profiles to a predefined target profile at some time instant T within the time window $[T_1, T_2]$ in the flattop phase (color online)

*supported partially by the US NSF CAREER award program (ECCS-0645086), National Natural Science Foundation of China (No. F030119), Zhejiang Provincial Natural Science Foundation of China (Nos. Y1110354, Y6110751) and the Fundamental Research Funds for the Central Universities of China (No. 1A5000-172210101) and the Natural Science Foundation of Ningbo (No. 2010A610096)

of this problem aims at saving long trial-and-error periods of time currently spent by fusion experimentalists trying to manually adjust the time evolutions of the actuators to achieve the desired plasma profiles at some time instant during the early stage of the flattop phase [4]. As an alternative approach, the data-driven modeling technique has been applied to the area of current profile control, which does not fully use the models and parameters from the first principle of plasma physics, e.g., the results from JET [5~7], DIII-D [8] and the ASDEX Upgrade tokamaks [9].

We have recently proposed some advanced nonlinear optimization techniques (e.g., extremum-seeking [10] and sequential quadratic programming [11]) to solve this very challenging problem, and we have used them for the control of the current profile evolution during the ramp-up phase of discharge in the DIII-D tokamak. Instead of solving the PDE-constrained optimization problem, which is often computationally costly, we can interpolate the transient dynamics by connecting the initial to the desired final profiles. By choosing two feasible curves satisfying the spatial boundary conditions to connect the initial to the desired final profiles at both boundary points, an optimal surface spanned by the four-edge frame (two boundary curves, initial and desired final profiles, see Fig. 2) can be obtained by solving a 2-D nonlinear elliptical PDE arising from the minimal surface theory in differential geometry (see, e.g., Refs. [12,13]). This surface, which represents the desired transient dynamics, satisfies the boundary conditions and minimizes the dynamic fluctuations. Thus, the ramp-up-phase final-time optimal control problem becomes a trajectory tracking problem. The computational optimal trajectories can be directly implemented to the current profile control but it can not attenuate external noises and the errors driven by the modeling uncertainties. Thus, feedback control should be used to enhance the system robustness. Besides the feedback control synthesis based on the data-driven identification models in Refs. [5~7], the robust optimal control approach [14] has been applied to the current profile control at DIII-D [15~18].

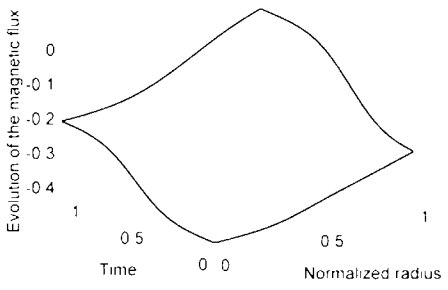

Fig.2 The four-edge frame including the initial magnetic flux distribution $\psi(\hat{\rho}, t_0)$ and the desired target magnetic flux distribution $\psi^{\mathrm{d}}(\hat{\rho})$ at the final time t_{f}. At the boundary $\hat{\rho} = 0$ and $\hat{\rho} = 1$, we connect $\psi_0(0)$ and $\psi^{\mathrm{d}}(0)$ to generate smooth transient dynamics for $\psi(0, t)$, and $\psi_0(1)$ and $\psi^{\mathrm{d}}(1)$ to generate smooth transient dynamics for $\psi(1, t)$ (color online)

Knowing the desired temporal-spatial evolutions, both spatial and temporal derivatives of the distributed profiles can be computed. Thus, at each time instant the transport PDEs degenerate to algebraic equations at every spatial point where the control values are the only unknowns. Optimization problems can be formulated to solve the algebraic equations by taking into account the control constraints (see, e.g., Refs. [19,20]). By using this proposed technique, the ramp-up current profile optimal control problem can be formulated into a least-square problem with algebraic constraints, which is much less computationally demanding.

The paper is organized as follows. The optimal control problem for the current profile system is introduced in section 2. The transient dynamics defined by the minimal surface theory is presented in section 3. In section 4, algebraic equations for the unknown control values are formulated at each time instant and are later solved by the least square method. Simulation studies are presented in section 5. The paper is closed in section 6 by stating conclusions and future research remarks.

2 Statement of the control problem

2.1 Control-oriented model

Dynamics of tokamak fusion plasmas is quite complicated and the main reason is the coupling between various physical responses of different time scales. In addition to the accuracy of actuators, the discrepancies between the desired control trajectories and the actual ones are unavoidable. Thus, compensation based on advanced control techniques is needed to enhance the robustness. To enable model-based control of the current profile at DIII-D, a control-oriented model for the dynamic evolution of the poloidal flux profile during and just after the ramp-up of the plasma current has been recently proposed [21]. During "Phase I" (see Fig. 1), mainly governed by the ramp-up phase, the plasma current is mostly driven by induction. In this case, it is possible to decouple the equation for the evolution of the poloidal flux $\psi(\hat{\rho}, t)$ from the equation for the evolution of the temperature $T_{\mathrm{e}}(\hat{\rho}, t)$. The magnetic diffusion equation is combined with empirical correlations obtained at DIII-D for the temperature and non-inductive current to introduce a simplified dynamic model describing the evolution of the poloidal flux during the inductive phase of the discharge. The technique using separation of time scales has been already applied to the current profile control of tokamak fusion plasmas, such as JET [4~6] and DIII-D [10,21].

The current density j, that flows toroidally around the tokamak and whose profile must be controlled, is related to spatial derivatives of the poloidal magnetic flux ψ. We let ρ be an arbitrary coordinate indexing the magnetic surface. Any quantity constant on each magnetic surface could be chosen as the variable ρ. We

choose the mean geometric radius of the magnetic surface as the variable ρ, i.e., $\pi B_{\phi,0}\rho^2 = \Phi$, where $B_{\phi,0}$ is the reference toroidal magnetic field at the geometric plasma center R_0. The variable $\hat{\rho}$ denotes the normalized radius $\frac{\rho}{\rho_{\rm b}}$, and $\rho_{\rm b}$ is the radius of the last closed flux surface. The evolution of the poloidal flux in normalized cylindrical coordinates is given by the magnetic diffusion equation,

$$\frac{\partial\psi}{\partial t} = \frac{\eta(T_{\rm e})}{\mu_0\rho_{\rm b}^2\hat{F}^2}\frac{1}{\hat{\rho}}\frac{\partial}{\partial\hat{\rho}}\left(\hat{\rho}\hat{F}\hat{G}\hat{H}\frac{\partial\psi}{\partial\hat{\rho}}\right) - R_0\hat{H}\eta(T_{\rm e})\frac{<\bar{j}_{\rm NI}\cdot\bar{B}>}{B_{\phi,0}}, \quad (1)$$

where t is the time, ψ is the poloidal magnetic flux, η is the plasma resistivity, $T_{\rm e}$ is the plasma electron temperature, μ_0 is the vacuum permeability, $\bar{j}_{\rm NI}$ is the non-inductive source of current density (neutral beam, electron cyclotron, etc.), $\bar{B}$ is the toroidal magnetic field, and $<>$ denotes flux-surface average. $\hat{F}$, $\hat{G}$, $\hat{H}$ are geometric factors, which are functions of $\hat{\rho}$, independent of the time variable for a given magnetic equilibrium. The boundary conditions of Eq. (1) are given by

$$\left.\frac{\partial\psi}{\partial\hat{\rho}}\right|_{\hat{\rho}=0} = 0, \left.\frac{\partial\psi}{\partial\hat{\rho}}\right|_{\hat{\rho}=1} = \frac{\mu_0}{2\pi}\frac{R_0}{\hat{G}\Big|_{\hat{\rho}=1}\hat{H}\Big|_{\hat{\rho}=1}}I(t), \quad (2)$$

where $I(t)$ denotes the total plasma current.

Highly simplified models for the temperature and non-inductive toroidal current density are chosen for the inductive phase of the discharge. Based on experimental observations at DIII-D, the shapes of the profiles are assumed to remain fixed and equal to the so-called reference profiles, which are identified from DIII-D discharges associated with the experiment of interest. The responses to the actuators are simply scalar multiples of the reference profiles.

The temperature $T_{\rm e}$ is assumed to follow

$$T_{\rm e}(\hat{\rho},t) = k_{T\rm e}T_{\rm e}^{\rm profile}(\hat{\rho})\frac{I(t)\sqrt{P}}{\bar{n}(t)}, \quad (3)$$

where the reference profile $T_{\rm e}^{\rm profile}$ is identified from DIII-D through Thomson scattering, and $k_{T\rm e} = 1.7295\times10^{10}\ \mathrm{m^{-3}A^{-1}W^{-1/2}}$. The average density $\bar{n}$ is defined as $\bar{n}(t) = \int_0^1 n(\hat{\rho},t)\mathrm{d}\hat{\rho}$, where n denotes the plasma density and P the total power of non-inductive current drive.

The non-inductive toroidal current density $\frac{<\bar{j}_{\rm NI}\cdot\bar{B}>}{B_{\phi,0}}$ is assumed to follow

$$\frac{<\bar{j}_{\rm NI}\cdot\bar{B}>}{B_{\phi,0}} = k_{\rm NIpar}j_{\rm NIpar}^{\rm profile}(\hat{\rho})\frac{I(t)^{1/2}P(t)^{5/4}}{\bar{n}(t)^{3/2}}, \quad (4)$$

where the reference profile $j_{\rm NIpar}^{\rm profile}$ is identified from DIII-D through a combination of MSE (motional Stark effect [22]) diagnostics and the EFIT equilibrium reconstruction code [23,24], and $k_{\rm NIpar} = 1.2139\times10^{18}\ \mathrm{m^{-9/2}A^{-1/2}W^{-5/4}}$. The model for $T_{\rm e}$ and $\frac{<\bar{j}_{\rm NI}\cdot\bar{B}>}{B_{\phi,0}}$ presented above considers neutral beams as the only source of current and heating. In the case where more heating and current sources are considered, Eqs. (3) and (4) should include the weighted contributions of the different sources, and reference profiles need to be identified for each heating and current source. The resistivity η scales with the temperature $T_{\rm e}$ as $\eta(\hat{\rho},t) = \frac{k_{\rm eff}Z_{\rm eff}}{T_{\rm e}^{3/2}(\hat{\rho},t)}$, where $Z_{\rm eff} = 1.5$, and $k_{\rm eff} = 4.2702\times10^{-8}\ \Omega\cdot\mathrm{m}\cdot(\mathrm{keV})^{3/2}$. By introducing

$$\vartheta_1(\hat{\rho}) = \frac{k_{\rm eff}Z_{\rm eff}}{k_{T\rm e}^{3/2}\mu_0\rho_{\rm b}^2}\frac{1}{\hat{F}^2(\hat{\rho})\left(T_{\rm e}^{\rm profile}(\hat{\rho})\right)^{3/2}},$$
$$D(\hat{\rho}) = \hat{F}\hat{G}\hat{H},$$
$$\vartheta_2(\hat{\rho}) = R_0\hat{H}\mu_0\rho_{\rm b}^2\hat{F}^2(\hat{\rho})k_{\rm NIpar}j_{\rm NIpar}^{\rm profile}(\hat{\rho}),$$
$$k = \frac{\mu_0}{2\pi}\frac{R_0}{\hat{G}(1)\hat{H}(1)},$$

the normalized poloidal magnetic flux can be rewritten as

$$\frac{1}{\vartheta_1(\hat{\rho})}\frac{\partial\psi}{\partial t} = u_1(t)\frac{1}{\hat{\rho}}\frac{\partial}{\partial\hat{\rho}}\left[\hat{\rho}D(\hat{\rho})\frac{\partial\psi}{\partial\hat{\rho}}\right] - \vartheta_2(\hat{\rho})u_2(t). \quad (5)$$

All the parameters mentioned above are listed in Table 1. The control inputs u_1 and u_2 are functions of physical actuators such as the total power P of the non-inductive current drive, the total plasma current I, and the average density $\bar{n}$, i.e.,

$$u_1(t) = \bar{n}^{1.5}I^{-1.5}P^{-0.75}, \quad u_2(t) = P^{0.5}I^{-1}. \quad (6)$$

Table 1. A description of the parameters

Parameters	Description
ψ	Poloidal flux
$\eta(T)$	Plasma resistivity
$T_{\rm e}$	Electron temperature
n	Plasma density
$\mu_0 = 4\pi\times10^{-7}(\frac{\rm H}{\rm m})$	Vacuum permeability
$\rho_{\rm b} = 0.79\ (m)$	Radius of last closed flux surface
$\Psi_{\rm b}$	Toroidal flux in the last closed flux surface
$B_{\phi,0} = 1.85$ (T)	Reference magnetic field at R_0
$R_0 = 1.668$ (m)	Reference point for $B_{\phi,0}$ (e.g., geometric center of plasma $R_{\rm geo}$)
$\hat{\rho}$	Normalized radius $\frac{\rho}{\rho b}$
$\hat{F},\hat{G},\hat{H}$	Geometric factors
$\bar{j}_{\rm NI}$	Any non-inductive source of current density (neutral beam, electron cyclotron, etc.)
$<>$	Flux-surface average
j	Toroidal current density
E	Toroidal electric field
σ	Plasma conductivity
I	Total plasma current
$P_{\rm tot}$	Total power of non-inductive current drive
$\bar{n}$	Spatially average density

The poloidal magnetic flux at the spatial boundaries is determined by the Neumann conditions

$$\frac{\partial\psi}{\partial\hat{\rho}}(0,t) = 0, \quad \frac{\partial\psi}{\partial\hat{\rho}}(1,t) = ku_3(t), \quad u_3(t) = I, \quad (7)$$

where k is a constant. The initial condition for the magnetic flux profile is given by $\psi(\hat{\rho},t_0)=\psi_0(\hat{\rho})$.

This proposed method takes advantage of the time scale discrepancies between various physical variables, mainly the normalized poloidal magnetic flux $\psi(\hat{\rho},t)$ and the temperature profile $T_{\rm e}(\hat{\rho},t)$, by neglecting the time evolution of $T_{\rm e}(\hat{\rho},t)$ and replacing it by a rigid empirical relationship (i.e., without considering the response delays in Eqs. (3) and (4), respectively). A further combination of the current quasi-static assumption and the sequential update of the magnetic equilibrium is needed when the evolution of equilibrium at the initial current ramp up phase is not negligible.

2.2 Cost functional and constraints

In practice, the toroidal current density is usually specified indirectly by the safety factor which is defined as $q(\hat{\rho},t)=\left[\frac{\partial\psi}{\partial\hat{\rho}}\right]^{-1}B_{\phi,0}\rho_{\rm b}^2\hat{\rho}=\left[\frac{\partial\psi(\rho,t)}{\partial\Phi}\right]^{-1}$. The constant relationship between Φ and ρ, $\rho=\sqrt{\frac{\Phi}{\pi B_{\phi,0}}}$. The control objective is to find control inputs $P(t)$ and $I(t)$ that minimize the cost functional

$$J=\frac{1}{2}\int_0^1\left|q(\hat{\rho},t_{\rm f})-q^{\rm d}(\hat{\rho})\right|^2{\rm d}\hat{\rho}$$
$$+\frac{1}{2}\int_{t_0}^{t_{\rm f}}\left(\gamma_I I^2+\gamma_P P^2+\gamma_{\bar{n}}\bar{n}^2\right){\rm d}t,$$

where $q^{\rm d}(\hat{\rho})$ is the desired target profile at time $t_{\rm f}$, and the positive constants γ_I, γ_P and $\gamma_{\bar{n}}$ are control weighting factors. The control actuators may need to satisfy constraints such as:

$$\text{Magnitude saturation}: \left(\begin{array}{c} I_{\rm l}^{(0)}\le I\le I_{\rm u}^{(0)},\\ P_{\rm l}\le P\le P_{\rm u}\\ \bar{n}_{\rm l}\le\bar{n}\le\bar{n}_{\rm u}\end{array}\right); \quad (8)$$

$$\text{Rate saturation}: \left|\frac{{\rm d}I(t)}{{\rm d}t}\right|\le I_{\rm u}^{(1)}; \quad (9)$$

$$\text{Initial and final values}: I(t_0)=I_0,\ I(t_{\rm f})=I_{\rm f}, \quad (10)$$

where $I_{\rm l}^{(0)}$ and $I_{\rm u}^{(0)}$ represent the lower and upper bounds of the current actuation function $I(t)$ while $I_{\rm u}^{(1)}$ represent the upper bound of rate. $P_{\rm l}$ and $P_{\rm u}$ represent the lower and upper bounds of the total power. $\bar{n}_{\rm l}$ and $\bar{n}_{\rm u}$ represent the lower and upper bounds of the line average density. This is set to prevent density instabilities and disruptions. The upper limit of the line average density is approximately half of the Greenwald limit at DIII-D. More interestingly, we have fixed starting and ending values (I_0 and $I_{\rm f}$, respectively) for the current actuation function.

The waveforms generated by the proposed optimization algorithm in this work are the references for the controllers associated with the plasma current $I(t)$, line averaged density $\bar{n}(t)$, and beam power $P(t)$. In the case of the plasma current, a PID loop regulates the ohmic coil voltage $V_{\rm loop}$ at DIII-D to make the plasma current measured by a Rogowski loop (which includes both inductive and non-inductive current components) follow the desired waveform generated by the optimization algorithm. Similarly, a PID loop regulates gas puffing and pumping to make the line averaged density measured by a CO_2 interferometer follow the optimal waveform. The power of the current drive is directly controlled by the power supplies associated with the drive. Recent experiments in DIII-D have shown the possibility of controlling both plasma current and beam power very accurately. However, the control of the evolution of the line average density appears as more challenging.

3 Transient dynamics design

3.1 Edge design

By noting $\frac{\partial\psi}{\partial\hat{\rho}}=\frac{1}{q(\hat{\rho},t)}B_{\phi,0}\rho_{\rm b}^2\hat{\rho}$ and naturally holding $\frac{\partial\psi}{\partial\hat{\rho}}(\hat{\rho}=0,t)=0$, a desired target magnetic flux profile at the final time $t_{\rm f}$, i.e. $\psi(\hat{\rho},t_{\rm f})=\psi^{\rm d}(\hat{\rho})$, can be obtained by integrating the desired output $q^{\rm d}(\hat{\rho})$ over $[0,\hat{\rho}]$, $(0\le\hat{\rho}\le1)$:

$$\psi^{\rm d}(\hat{\rho})=\psi^{\rm d}(0)+\int_0^{\hat{\rho}}\frac{1}{q^{\rm d}(\varrho)}B_{\phi,0}\rho_{\rm b}^2\varrho{\rm d}\varrho, \quad (11)$$

where either $\psi^{\rm d}(0)$ or $\psi^{\rm d}(1)$ need to be fixed to obtain the desired $\psi^{\rm d}$-curve shown in Fig. 2. We can determine the left $(\psi(0,t_0)\ \psi(0,t_{\rm f}))$ and right $(\psi(1,t_0),\ \psi(1,t_{\rm f}))$ boundary values by using the compatibility conditions: $\psi(0,t_0)=\psi_0(0)$, $\psi(1,t_0)=\psi_0(1)$, $\psi(0,t_{\rm f})=\psi^{\rm d}(0)$ and $\psi(1,t_{\rm f})=\psi^{\rm d}(1)$. Thus, we add a sequence of points $\{\psi(0,T_i)\}_{i=1}^{I},T_i\in(t_0,t_{\rm f})$, between $\psi(0,t_0)$ and $\psi(0,t_{\rm f})$, and a sequence of points $\{\psi(1,T_j)\}_{j=1}^{J},T_j\in(t_0,t_{\rm f})$, between $\psi(1,t_0)$ and $\psi(1,t_{\rm f})$ to represent the left and right boundary evolution conditions (Dirichlet boundary conditions) via spline interpolations. Therefore, we obtain the four-edge frame shown in Fig. 2, where the surface within this frame representing the desired transient dynamics still needs to be defined.

3.2 Minimal surface

In Fig. 3, we define $\mathcal{M}=\{0\le\hat{\rho}\le1,t_0\le t\le t_{\rm f}\}$ in the $\hat{\rho}t$-plane with the boundary denoted by $\partial\mathcal{M}$. We define a three dimensional curve $\partial S\triangleq E\frown F\frown G\frown H\frown E$ over $\partial\mathcal{M}$, which can span a surface S in infinite ways. In this work, the minimal surface theory is used to define a unique surface within the frame and minimize transient fluctuations. We discuss the detailed theory and algorithms in the rest of this subsection. Besides the minimal surface theory, other approaches such as the spline interpolation surface methods can be also used to construct the transient dynamics. The construction of transient dynamics can utilize the priori experience from historic data to achieve smooth transition in an off-line fashion.

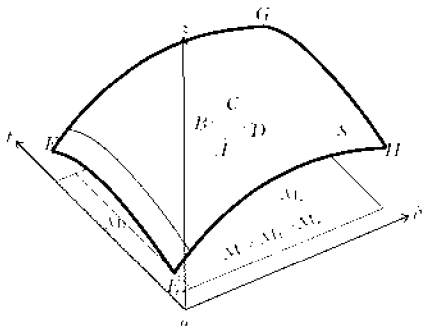

Fig.3 Surface integral. The surface S over domain $\mathcal{M}$ is expressed by $z = \psi(\hat{\rho}, t)$, $\forall(\hat{\rho}, t) \in \mathcal{M}$. The coordinate of A is $(\hat{\rho}_0, t_0, z_0)$, where $z_0 = \psi(\hat{\rho}_0, t_0)$. The coordinate of B is $(\hat{\rho}_0, t_0 + \mathrm{d}t, z_0 + \psi_t(\hat{\rho}_0, t_0)\mathrm{d}t)$, where $\psi_t(\hat{\rho}_0, t_0) = \frac{\partial \psi}{\partial t}(\hat{\rho}_0, t_0)$, and $\mathrm{d}t$ is the length of the line element $\overline{AB}$ on the t-o-$\hat{\rho}$ plane. The coordinate of D is $(\hat{\rho}_0 + \mathrm{d}\hat{\rho}, t_0, z_0 + \psi_{\hat{\rho}}(\hat{\rho}_0, t_0)\mathrm{d}\hat{\rho})$, where $\psi_{\hat{\rho}}(\hat{\rho}_0, t_0) = \frac{\partial \psi}{\partial \hat{\rho}}(\hat{\rho}_0, t_0)$, and $\mathrm{d}\hat{\rho}$ is the length of the line element $\overline{AD}$ on the t-o-$\hat{\rho}$ plane. Then, the vector $\vec{AB}$ is $(0, \mathrm{d}t, \psi_t(\hat{\rho}_0, t_0)\mathrm{d}t)$ and the vector $\vec{AD}$ is $(\mathrm{d}\hat{\rho}, 0, \psi_{\hat{\rho}}(\hat{\rho}_0, t_0)\mathrm{d}\hat{\rho})$. Therefore, the area of the element $\square ABCD$ is $\left|\vec{AB} \times \vec{AD}\right|$ $= |(-\psi_{\hat{\rho}}(\hat{\rho}_0, t_0)\mathrm{d}\hat{\rho}\mathrm{d}t, -\psi_t(\hat{\rho}_0, t_0)\mathrm{d}\hat{\rho}\mathrm{d}t, \mathrm{d}\hat{\rho}\mathrm{d}t)|$ $= \sqrt{1 + \psi^2_{\hat{\rho}}(\hat{\rho}_0, t_0) + \psi^2_t(\hat{\rho}_0, t_0)}\mathrm{d}\hat{\rho}\mathrm{d}t$ (color online)

We use $z = \psi(\hat{\rho}, t)$ to express the surface S. As shown in Fig. 3, the minimal surface problem can be stated as the following optimization problem:

$$\min_{\psi(\hat{\rho},t)} \iint_M \sqrt{1 + \psi^2_{\hat{\rho}}(\hat{\rho}, t) + \psi^2_t(\hat{\rho}, t)}\mathrm{d}\hat{\rho}\mathrm{d}t, \tag{12}$$

$$\text{subject to: } \psi(\hat{\rho}, t)|_{\partial\mathcal{M}} = g(\hat{\rho}, t) \triangleq$$

$$\begin{cases} \psi_0(\hat{\rho}), & \hat{\rho} \in [0,1],\ t = t_0, \\ \mathrm{Spline}\left(\psi(0,t_0), \{\psi(0,T_i)\}_{i=1}^{I}, \psi(0,t_{\mathrm{f}})\right),\ T_i \in (t_0, t_{\mathrm{f}}), \\ \mathrm{Spline}\left(\psi(1,t_0), \{\psi(1,T_j)\}_{j=1}^{J}, \psi(1,t_{\mathrm{f}})\right),\ T_j \in (t_0, t_{\mathrm{f}}), \\ \psi^{\mathrm{d}}(\hat{\rho}), & \hat{\rho} \in [0,1],\ t = t_{\mathrm{f}}, \end{cases}$$

where $\partial\mathcal{M}$ is the boundary of the domain $\mathcal{M}$ and satisfies $\partial\psi(\hat{\rho}, t)/\partial\hat{\rho}|_{\hat{\rho}=0} = 0$. There are very few examples of minimal surfaces that can be expressed analytically. Nonlinear programming (NLP) can be used in general to find a numerical solution minimizing the area functional, but it is often computationally costly. Alternatively, by using the Euler-Lagrange equation in the calculus of variations [13], the minimal surface problem (12) can be reformulated as a nonlinear elliptic PDE:

$$\frac{\partial}{\partial\hat{\rho}}\left(\frac{\psi_{\hat{\rho}}}{\sqrt{1 + \psi^2_{\hat{\rho}} + \psi^2_t}}\right) + \frac{\partial}{\partial t}\left(\frac{\psi_t}{\sqrt{1 + \psi^2_{\hat{\rho}} + \psi^2_t}}\right) = 0,$$

$$\psi(\hat{\rho}, t)|_{\partial\mathcal{M}} = g(\hat{\rho}, t). \tag{13}$$

This is called the minimal surface equation, which is impossible to solve analytically in general and numerical algorithms such as the finite element method (FEM) [25] or the finite difference method (FDM) [26] can be used to obtain numerical solutions.

One challenge arising from the implementation of the minimal surface theory for the definition of the transient dynamics of the magnetic flux is the satisfaction of the boundary conditions. In this problem, a Neumann boundary condition at $\hat{\rho} = 0$ must be satisfied. However, such a spatial derivative requirement is not taken into account by the minimal surface Eq. (13). To overcome this challenge, we decompose the domain into sub-domains and solve the minimal surface equation (nonlinear elliptic PDE) over each sub-domain with overlapping boundaries. In order to define a transient dynamics satisfying the zero Neumann boundary condition at $\hat{\rho} = 0$, we split the domain into two sub-domains $\mathcal{M} = \mathcal{M}_1 \cup \mathcal{M}_2$, where $\mathcal{M}_1$ is a narrow region of width $\bar{\Delta}\hat{\rho}$ along the $\hat{\rho} = 0$ boundary (Fig. 3). By properly defining the Dirichlet boundary conditions for $\mathcal{M}_1$, it is possible to approximately satisfy the zero Neumann boundary condition at $\hat{\rho} = 0$.

4 Control computations

4.1 Scalar analysis

In plasma discharge experiments at the DIII-D tokamak, the total power $P(t)$, the total plasma current $I(t)$, and the average density $\bar{n}(t)$ are of order 10^6 W, 10^6 A, and 10^{19} m^{-3} respectively. The coefficients $\vartheta_1(\hat{\rho})$ and $\vartheta_2(\hat{\rho})$, which vary with respect to $\hat{\rho}$, are of order 10^{-15} and 10^{13}, respectively. The poloidal magnetic flux $\psi(\hat{\rho}, t)$, which varies with respect to both the normalized radius and time, is of order 10^{-1}. The other variables in Eq. (5) are of order 1. Thus, we can estimate the orders of all the terms in Eqs. (5) and (6): $\frac{1}{\vartheta_1(\hat{\rho})}\frac{\partial\psi}{\partial t} \sim 10^{14}$, $u_1(t) \sim 10^{15}$, $u_1(t)\frac{1}{\hat{\rho}}\frac{\partial}{\partial\hat{\rho}}\left[\hat{\rho}D(\hat{\rho})\frac{\partial\psi}{\partial\hat{\rho}}\right] \sim 10^{14}$, $u_2(t) \sim 10^{-3}$ and $\vartheta_2(\hat{\rho})u_2(t) \sim 10^{10}$. Therefore, the interior control term $\vartheta_2(\hat{\rho})u_2(t)$ is small in comparison to other terms in Eq. (5).

4.2 Least square scheme

We consider a grid division $(\hat{\rho}_i, t_j)$ in the temporal-spatial domain $\mathcal{M} = \{0 \le \hat{\rho} \le 1, 0 \le t \le t_{\mathrm{f}}\}$: $0 = \hat{\rho}_1 < \hat{\rho}_2 < \ldots < \hat{\rho}_i < \ldots < \hat{\rho}_M = 1$ and $t_0 = t_1 < t_2 < \ldots < t_j < \ldots < t_N = t_{\mathrm{f}}$. We assume that the desired transient dynamics is obtained by solving the minimal surface Eq. (13) and is denoted by $\tilde{\psi}(\hat{\rho}, t)$ over $\mathcal{M}$. Then, we can compute the boundary control through the Neumann boundary condition (7), $u_3(t_n) = \frac{1}{k}\frac{\partial\tilde{\psi}}{\partial\hat{\rho}}(1, t_n)$, $n = 1, 2, \ldots, N$.

Based on the results of our order analysis, we let the interior control $u_2 = 10^{-3}$ and rewrite the PDE system (5) as the following linear system

$$\frac{1}{\hat{\rho}}\frac{\partial}{\partial\hat{\rho}}\left[\hat{\rho}D(\hat{\rho})\frac{\partial\psi}{\partial\hat{\rho}}\right]u_1(t) = \frac{1}{\vartheta_1(\hat{\rho})}\frac{\partial\psi}{\partial t} + \vartheta_2(\hat{\rho})u_2(t), \tag{14}$$

where u_1 must be obtained at t_n, $n = 1, 2, \ldots, N$. For each t_n, $n = 1, 2, \ldots, N$, Eq. (14) can be satisfied at

each spatial node $\hat{\rho}_m$, $m = 2, 3, \ldots, M$, i.e.,

$$A^n_{2,M} u_1(t_n) = b^n_{2,M}, n = 1, 2, \ldots, N, \tag{15}$$

where

$$A^n_{2,M} = \begin{pmatrix} \frac{1}{\hat{\rho}_2}\frac{\partial}{\partial\hat{\rho}}\left[\hat{\rho}D(\hat{\rho})\frac{\partial\tilde{\psi}(\hat{\rho}_2,t_n)}{\partial\hat{\rho}}\right] \\ \vdots \\ \frac{1}{\hat{\rho}_M}\frac{\partial}{\partial\hat{\rho}}\left[\hat{\rho}D(\hat{\rho})\frac{\partial\tilde{\psi}(\hat{\rho}_M,t_n)}{\partial\hat{\rho}}\right] \end{pmatrix}, \tag{16}$$

$$b^n_{2,M} = \begin{pmatrix} \frac{1}{\vartheta_1(\hat{\rho}_2)}\frac{\partial\tilde{\psi}(\hat{\rho}_2,t_n)}{\partial t} + \vartheta_2(\hat{\rho}_2)u_2(t_n) \\ \vdots \\ \frac{1}{\vartheta_1(\hat{\rho}_M)}\frac{\partial\tilde{\psi}(\hat{\rho}_M,t_n)}{\partial t} + \vartheta_2(\hat{\rho}_M)u_2(t_n) \end{pmatrix}. \tag{17}$$

Without considering any actuation constraint, we can obtain the least square solution of the linear system (15) as

$$u^n_1 = u_1(t_n) = \left\{\left[A^n_{2,\mathrm{M}}\right]^T A^n_{2,M}\right\}^{-1}\left[A^n_{2,M}\right]^T b^n_{2,M}. \tag{18}$$

In general, we can formulate the following optimization problem in the presence of actuation constraints:

$$\min_{\mathbf{u}_1\in\mathcal{U}} \frac{1}{2}\beta_1\|\mathbf{u}_1\|^2 + \frac{1}{2}\sum_{n=1}^{N}\beta_{2,n}\left\|A^n_{2,M}u_1(t_n) - b^n_{2,M}\right\|^2, \tag{19}$$

where $\mathbf{u}_1 = (u_1(t_1), \ldots, u_1(t_n), \ldots, u_1(t_\mathrm{f}))^T$, β_1 and $\beta_{2,n}$ are positive weighting constants and $\mathcal{U}$ is the admissible control set defined by Eqs. (8)$\sim$(10) at $t = t_n$, $n = 1, 2, \ldots, N$. This is a quadratic programming problem which can be solved relatively quickly.

4.3 Computational derivatives

The matrices in Eq. (15) include both the temporal and spatial derivatives of the desired transient dynamics $\tilde{\psi}(\hat{\rho}, t)$ over $\mathcal{M}_{m,n} = (\hat{\rho}_m, t_n)$, $m = 1, 2, \ldots, M$ and $n = 1, 2, \ldots, N$. Using the discrete values $\tilde{\psi}(\hat{\rho}_{m-1}, t_n)$, $\tilde{\psi}(\hat{\rho}_m, t_n)$ and $\tilde{\psi}(\hat{\rho}_{m+1}, t_n)$ defined on a uniform grid, we can obtain the spatial second-order difference formulas:

$$\frac{\partial\tilde{\psi}}{\partial\hat{\rho}}(\hat{\rho}_1, t_n) \approx \frac{-3\tilde{\psi}(\hat{\rho}_1, t_n) + 4\tilde{\psi}(\hat{\rho}_2, t_n) - \tilde{\psi}(\hat{\rho}_3, t_n)}{2\Delta\hat{\rho}},$$

$$\frac{\partial\tilde{\psi}}{\partial\hat{\rho}}(\hat{\rho}_m, t_n) \approx \frac{\tilde{\psi}(\hat{\rho}_{m+1}, t_n) - \tilde{\psi}(\hat{\rho}_m, t_n)}{2\Delta\hat{\rho}}, \quad m \in [2, M-1],$$

$$\frac{\partial\tilde{\psi}}{\partial\hat{\rho}}(\hat{\rho}_M, t_n) \approx \frac{\tilde{\psi}(\hat{\rho}_{M-2}, t_n) - 4\tilde{\psi}(\hat{\rho}_{M-1}, t_n) + 3\tilde{\psi}(\hat{\rho}_M, t_n)}{2\Delta\hat{\rho}},$$

where $\Delta\hat{\rho}$ is the spatial step length. The term $\frac{1}{\hat{\rho}}\frac{\partial}{\partial\hat{\rho}}\left[\hat{\rho}D(\hat{\rho})\frac{\partial\tilde{\psi}(\hat{\rho}_m,t_n)}{\partial\hat{\rho}}\right]$ is computed using similar second-order difference formulas in terms of the previously obtained $\frac{\partial\tilde{\psi}(\hat{\rho}_m,t_n)}{\partial\hat{\rho}}$ for $m = 1, 2, \ldots, M$. The temporal difference formulas are obtained following an identical procedure.

5 Numerical example

The geometrical parameters $D(\hat{\rho})$, $\vartheta_1(\hat{\rho})$ and $\vartheta_2(\hat{\rho})$ in model (5) are shown in Fig. 4, which are identified from experimental data. Given the initial and desired profiles of the magnetic flux $\psi(\hat{\rho}, t)$ in Fig. 5, we use splines to define the boundary evolutions over $\partial\mathcal{M}$, which are shown in Fig. 6. This formulates a four-edge frame without giving the detailed transient dynamics. The minimum surface theory is proposed in this work to generate a smooth dynamic evolution incorporating priori experimental experience and constraints. However, it is not necessarily feasible to find a unique surface minimizing the area functional of the surface spanned by a general framework according to the differential geometry theory. Thus, in this work we make domain decompositions to obtain sub-patches and implement minimum surfaces over each patch. For example, we decompose the whole time-space domain into two subdomains $\mathcal{M}_1$ and $\mathcal{M}_2$, as shown in Fig. 7. Alternatively, spline interpolation of surfaces is also a good method to the surface generation but it requires more control points over the domain compared to the minimum surface theory. We generate a triangular grid division over the domain $\mathcal{M} = \mathcal{M}_1 \cup \mathcal{M}_2$, as shown in Fig. 7. Then, we use the finite element method to solve the minimal surface equation over both $\mathcal{M}_1$ and $\mathcal{M}_2$. We solve the minimal surface Eq. (13) over the discrete nodes in both $\mathcal{M}_1$ and $\mathcal{M}_2$ using the finite element method.

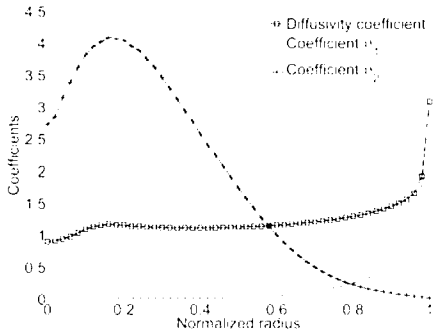

Fig.4 Diffusivity coefficient $D = \hat{F}\hat{G}\hat{H}$, coefficients $\vartheta_1(\times 10^{-15})$ and $\vartheta_2(\times 10^{13})$ versus the normalized radius $\hat{\rho}$ (color online)

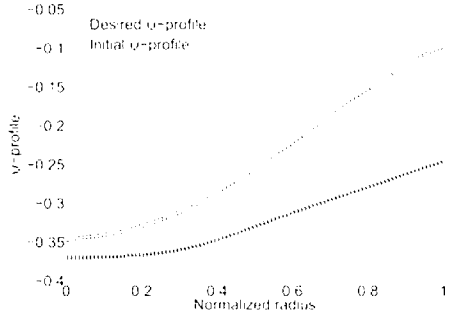

Fig.5 The initial and desired profiles (color online)

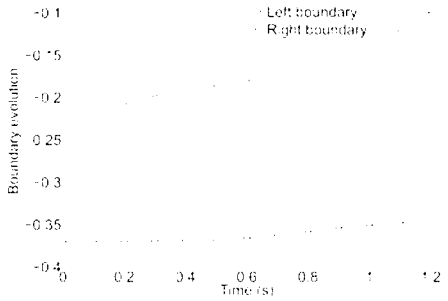

Fig.6 The left and right profiles (color online)

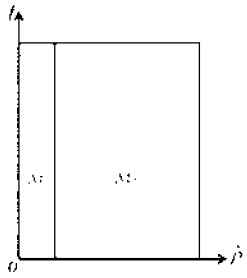

Fig.7 The triangular grid for FEM computations (color online)

In order to formulate the linear algebraic Eq. (15), we compute every term in Eq. (5) in terms of both the temporal and spatial derivatives using various finite difference schemes, which are shown in Fig. 8. Noting that $\frac{\partial \psi}{\partial \hat{\rho}}(\hat{\rho}=0,t)$ has a steep connection to 0 for all t in Fig. 8, then singularity (type-$\frac{0}{0}$) appears when computing the q-profile using the definition

$$q(\hat{\rho},t)=\frac{B_{\phi,0}\rho_{\mathrm{b}}^2\hat{\rho}}{\frac{\partial \psi}{\partial \hat{\rho}}}. \tag{20}$$

Therefore, the L'Hopital law has to be used to compute the q-profile at the origin, i.e.,

$$q(0,t)=\lim_{\hat{\rho}\to 0}\frac{B_{\phi,0}\rho_{\mathrm{b}}^2\hat{\rho}}{\frac{\partial \psi}{\partial \hat{\rho}}}=\lim_{\hat{\rho}\to 0}\frac{B_{\phi,0}\rho_{\mathrm{b}}^2}{\frac{\partial^2 \psi}{\partial \hat{\rho}^2}(\hat{\rho},t)}. \tag{21}$$

We obtain the control functions shown in Fig. 9 where we let $u_2(t)=10^{-3}$. Thus, we can obtain the physical actuators (denoted by P_{a}, I_{a} and n_{a}) taking into account the definitions (6) and (7). Using the obtained actuator functions, we simulate the PDE system (5) with boundary conditions (6). The obtained control functions can drive the system to the vicinity of the desired profile with a shape similar to the desired profile. This is illustrated in Fig. 10, where desired and actual flux profiles are compared to the initial profile. The error of ψ-profiles at the final time t_{f} seems to be rather constant with respect to space, which implies that the desired shape for the q-profile is achieved. Fig. 11 compares the desired q-profile with the actual q-profile at time t_{f}. As shown in Fig. 11, one can observe that the controlled q-profile at $t=t_{\mathrm{f}}$ has a much better match to the desired target over the interval $0.05\leq\hat{\rho}\leq 1$ and is sensitive over the interval $0\leq\hat{\rho}\leq 0.05$ due to

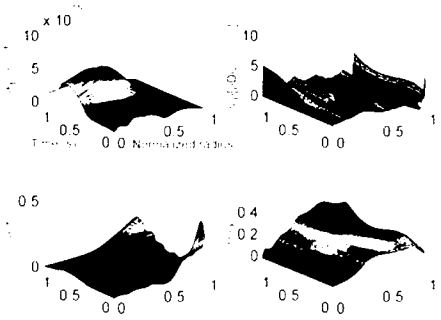

Fig.8 Computational derivative (color online)

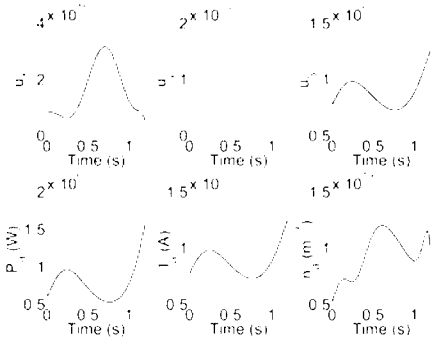

Fig.9 Computed control functions (color online)

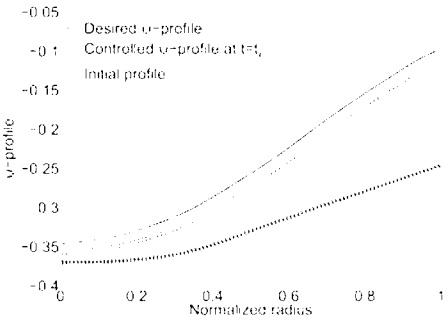

Fig.10 Controlled ψ profile (color online)

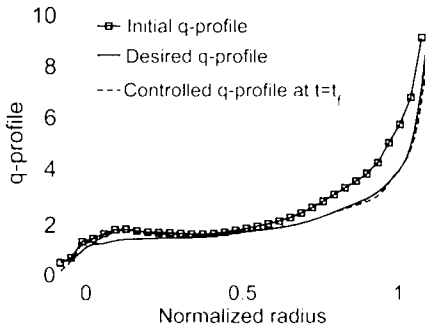

Fig.11 Controlled q-profile (color online)

boundary singularity compared to the initial q-profile. The explanation is that the PDE system (1)-(2) is a simplified model oriented for control that could not capture the exact physics on the boundaries but provides a good approximation within the interval. The rather constant flux error may be used to redefine $\psi^{\mathrm{d}}(0)$ (or $\psi^{\mathrm{d}}(1)$) during the definition of the desired magnetic flux target profile.

6 Conclusion

The open-loop finite-time optimal current profile control problem arising in tokamak plasmas during the ramp-up phase of the discharge is solved by using the minimal surface theory and the least square method (or the quadratic programming method when actuation constraints are taken into account). The minimal surface theory is used to generate the desired transient dynamics and then a tracking problem can be formulated for the current profile control. Knowing the transient dynamics, every term containing both temporal and spatial derivatives in the control-oriented PDE model can be computed using the finite difference method. Thus, the control-oriented PDE model becomes a set of algebraic equations where the only unknowns are the control functions at different instants of time.

Taking into account the control constraints, we can reformulate these algebraic equations as a quadratic programming problem. When no actuator constraint needs to be taken into account, the quadratic programming problem is simplified to a simple least square problem. Numerical studies demonstrate that this approach can significantly reduce computational effort, showing potential for real-time implementation in a closed-loop receding-horizon scheme, particularly for long-discharge tokamaks such as ITER.

Simulation results show that the numerical optimization procedure can generate control trajectories driving the final ψ-profile to the proximity of a predefined desired profile. Future work includes the implementation of this method directly in terms of the q variable in order to eliminate relatively spatially-constant matching errors that can appear in the ψ variable, which are indeed not important. Alternatively, an iterative scheme can be designed where the matching error is used to redefine the desired magnetic flux target profile, and therefore the transient dynamics, for the following iteration.

The quasi-static magnetic equilibrium assumption is used in this work and the update of equilibrium evolution can be incorporated directly in this framework. In the real experimental implementation, we also need to develop a feedback controller to track the nominal trajectory generated by the open-loop computation due to external noise and uncertainties. The PID control is the most popular model-free methodology used in practise and very easy to implement. When the computational trajectories are implemented in real experiments, PID controllers dynamically change the actuators to remain the optimal computational results.

Acknowledgements

The first author of this paper would like to extend his acknowledgement to Dr. Michael WALKER for his valuable comments to this paper.

References

1 Hinton F, Hazeltine R. 1976, Reviews of Modern Physics, 48: 239
2 Blum J. 1988, Numerical Simulation and Optimal Control in Plasma Physics. John Wiley & Sons, New York
3 Kokotovic P, Khali H K, OR' eilly J. 1999, Singular Perturbation Methods in Control: Analysis and Design. SIAM Press, New York
4 Witrant E, Joffrin E, Bremond S, et al. 2007, Plasma Physics and Controlled Fusion, 49: 1075
5 Moreau D, Crisanti F, Litaudon X, et al. 2003, Nuclear Fusion, 43: 870
6 Laborde L, Mazon D, Moreau D, et al. 2005, Plasma Physics and Controlled Fusion, 47: 155
7 Moreau D, Crisanti F, Litaudon X, et al. 2008, Nuclear Fusion, 48: 106001
8 Moreau D, Mazon D, Walker M, et al. 2011, Nuclear Fusion, 51: 063009
9 Na Y -S. 2003, Modelling of Current Profile Control in Tokamak Plasmas. Fakultat fur Physik: Technische Universitat Munchen
10 Ou Y, Xu C, Schuster E, et al. 2008, Plasma Physics and Controlled Fusion, 50: 115001
11 Xu C, Dalessio J, Ou Y, et al. 2008, Extremum-seeking open-loop control of plasma current profile at the DIII-D tokamak. Proceedings of the 2008 American Control Conference
12 Courant R. 1950, Dirichlet's Principle, Conformal Mapping, and Minimal Surfaces. Interscience Publishers, Inc., New York
13 Courant R, Hilbert D. 1953, Methods of Mathematical Physics. Interscience Publishers, Inc., New York
14 Zhou K, Doyle J. 1997, Essentials of Robust Control. Prentice Hall, New York
15 Xu C, Ou Y, Schuster E. 2011, Automatica, 47: 418
16 Ou Y, Xu C, Schuster E, et al. 2011, IEEE Transactions on Control Systems Technology, 19: 432
17 Barton J, Ou Y, Xu C, et al. 2011, Fusion Engineering and Design, 86: 1116
18 Barton J, Boyer M, Shi W, et al. 2012, Robust Control of the Current Profile Evolution During the Rampup and Early Flat-top Phases of the Plasma Discharge in the DIII-D Tokamak. Proceedings of the 2012 American Control Conference, Montreal, Canada, June 27~29, 2012
19 Boyd S, Vandenberghe L. 2004, Convex Optimization. Cambridge University Press, New York
20 Nocedal J, Wright S. 2006, Numerical Optimization. (2nd edition). Springer, New York
21 Ou Y, Xu C, Schuster E, et al. 2008, Plasma Physics & Controlled Fusion, 50: 115001
22 Hutchinson I. 2005, Principles of Plasma Diagnostics. (2nd edition). Cambridge University Press, New York
23 Lao L, John H, Stambaugh R, et al. 1985, Nuclear Fusion, 25: 1611
24 Ferron J, Walker M, Lao L, et al. 1998, Nuclear Fusion, 38: 1055
25 Ciarlet P. 1979, The Finite Element Method for Elliptic Problems. North-Holland, New York
26 Schiesser W. 1991, The Numerical Method of Lines. Academic Press, New York

(Manuscript received 24 February 2012)
(Manuscript accepted 11 July 2012)
E-mail address of XU Chao: cxu@zju.edu.cn